JOURNAL OF APPLIED ELECTROCHEMISTRY **26** (1996) 102–112

Kinetics and mechanism of the Al(III)/Al electrode reaction in cryolite–alumina melts

J. THONSTAD

Department of Electrochemistry, NTH, University of Trondheim, 7034 Trondheim, Norway

A. KISZA, J. KAZMIERCZAK

Institute of Chemistry, University of Wroclaw, 50-383 Wroclaw, Poland

Received 7 April 1995; revised 27 July 1995

Using the relaxation method (RM) with galvanostatic perturbation and electrochemical impedance spectroscopy (EIS), exchange current densities and activation parameters were determined for the electrode reaction on the aluminium electrode in pure cryolite melt and in cryolite–alumina melts with the addition of 2–12 wt % Al_2O_3. In all these melts a three step electrode process was observed, comprising a preceding chemical reaction followed by two charge transfer steps. The exchange current densities for two charge transfer steps were determined as a function of temperature, together with the equilibrium constant of the preceding chemical reaction and its kinetic and diffusion impedance. The third step was found to be independent of diffusion and of the concentration of alumina, whereas the second step showed mixed characteristics. The exchange current densities were of the order of 5–15 A cm^{-2}.

List of symbols

A	electrode area (cm^2)
A, B, C	coefficients of Equation 12 (V)
C_{dl}	double layer capacitance (F)
c	concentration (mol cm^{-3})
D_O, D_R	diffusion coefficients of the oxidized and reduced ionic species ($cm^2\ s^{-1}$)
E_A	activation energy (kJ mol^{-1})
F	Faraday constant (C mol^{-1})
j	exchange current density (A cm^{-2})
K	equilibrium constant (dimensionless)
k	sum of the forward (k_1) and backward (k_2) rate constants (s^{-1})
k_0	standard rate constant (cm s^{-1})
L_1, L_2	high frequency and low frequency inductances (H)
L_{out}	outer inductance (H)
R_{el}	electrolyte resistance (Ω)
n	number of electrons (dimensionless)
R	molar gas constant (J $mol^{-1}\ K^{-1}$)
R_{ct}	charge transfer resistance (Ω)
s_1, s_2	angular frequencies (s^{-1})
T	temperature (K)
t	time (s)
Z	complex impedance (Ω)
Z', Z''	real and imaginary parts of the complex impedance (Ω)
Z_w	Warburg diffusion impedance (Ω $s^{-1/2}$)

Greek symbols

α_c	overall cathodic transfer coefficient (dimensionless)
α, β	coefficients in Equation 12 ($s^{-1/2}$)
γ	coefficient in Equation 12 (s^{-1})
η	overpotential (V)
ω	angular frequency (s^{-1})
σ_O, σ_R	Warburg coefficients of the oxidized and reduced ionic species (Ω $s^{-1/2}$)

1. Introduction

Cryolite melts have a rather complex ionic structure. The classical model for cryolite dissociation is

$$Na_3AlF_6 = 3Na^+ + AlF_6^{3-} \quad (1)$$

$$AlF_6^{3-} = AlF_4^- + 2F^- \quad (2)$$

where the dissociation degree of pure cryolite (Equation 2) is approximately 0.25, and increases with decreasing NaF/AlF_3 molar ratio. This dissociation model is not universally accepted, as some authors claim that the AlF_5^{2-} ion is present [1]. The dissolved alumina forms binuclear oxyfluoride complexes of the type $Al_2OF_6^{2-}$ and $Al_2O_2F_4^{2-}$ [1]. In cryolite the alumina solubility amounts to about 20 mol % at around 1000 °C, while it decreases appreciably by addition of other fluorides, including AlF_3. In an alumina-saturated cryolite melt a large fraction of the aluminium fluoride complexes will be present in the form of oxyfluoride ions.

The transport number of the sodium ion in cryolite is close to unity [1]. The fact that sodium carries the current while aluminium is being deposited leads to

0021-891X/93

a shift towards higher NaF/AlF_3 ratios in the boundary layer at the cathode. E.m.f. data show that the aluminium electrode becomes increasingly negative when the NaF/AlF_3 ratio increases [1, 2], and this establishes a concentration overpotential during electrolysis. Concentration overpotential is the dominant cathodic overpotential on the aluminium electrode in cryolite melts, being of the order of 0.1 V at normal electrolysis current densities (0.4–0.8 A cm^{-2}).

However, there is also a small contribution of charge transfer overpotential. The first attempt to determine the charge transfer overpotential was due to Piontelli *et al.* [3], who found it to be only a few millivolts at normal current densities. Thonstad and Rolseth [2] applied the double pulse technique to determine the charge transfer overpotential in cryolite–alumina melts at 1010 °C. The product nj_0 was found to be equal to 36 A cm^{-2}, for example, for a one electron step the exchange current density was 36 A cm^{-2}, for a three electron step 12 A cm^{-2}. A similar result was obtained by impedance measurements [1, 2].

In our previous paper [4] an inductive model of the electric double layer in molten salts [5] was applied in the evaluation of the kinetic parameters of the aluminium electrode reaction in alumina saturated cryolite melt. A two-step electrode process was postulated:

$$AlF_4^- + 2e^- = AlF_{2(ads)}^- + 2F^- \qquad (3)$$

$$AlF_{2(ads)}^- + e^- = Al + 2F^- \qquad (4)$$

It was found that the second step (Equation 4) is not influenced by diffusion and its exchange current density (approximately 15 A cm^{-2} at 1010 °C) was determined by a combination of the relaxation and faradaic impedance methods (see below). The exchange current density of the first step (Equation 3), which is influenced by the diffusion of the depolarizer anion from the bulk of the melt and the kinetics of the preceding chemical reaction, was evaluated only on the basis of the recorded faradaic impedance spectra, as at that time, the theory of the relaxation method had not been extended to diffusive systems [6].

It is well known that if the value of the measured charge transfer resistance is below 1 Ω, and in this particular case it was below 0.1 Ω, the accuracy of the determination of the charge transfer resistance is limited [7]. It was, however, possible to draw an important conclusion from the values of exchange current densities of the first step (Equation 3). The exchange current densities of the first step in the melts studied [4], were found to be proportional to the overall mole fraction of the Al(III) ionic species, irrespective of its molecular composition. With the derivation of the relaxation theory for diffusive reversible electrode reactions [6] it becomes possible to evaluate this exchange current density more accurately and for variable alumina concentration in the cryolite melt. A possible chemical step, preceding the charge transfer, was not taken into account in the previous work [4]. In pure molten cryolite the preceding chemical step may simply be the dissociation of the AlF_6^{3-} anion:

$$AlF_6^{3-} \underset{k_2}{\overset{k_1}{\rightleftharpoons}} AlF_4^- + 2F^- \qquad (5)$$

whereas in cryolite–alumina containing melts the chemical step should involve oxyfluoride anions, for example:

$$Al_2OF_6^{2-} \underset{k_2}{\overset{k_1}{\rightleftharpoons}} Al_2OF_4 + 2F^- \qquad (6)$$

followed by a discharge step similar to Equation 3:

$$Al_2OF_4 + 2e^- \Longleftrightarrow AlF_{2(ads)}^- + AlOF_2^- \qquad (7)$$

The high frequency step (Equation 4) should be the same in both melts.

The measurements described below do not give any clue as to the nature of the intermediate species, and whereas Equation 5 seems to be an obvious choice for pure cryolite, the situation is much less clear in the presence of alumina. As shown in the following, the exchange current density of the second step (Equation 7) increases by addition of alumina, indicating that a different oxygen containing reactant is involved. However, the intermediate species suggested in Equations 6 and 7 should only be regarded as arbitrary examples.

2. Theory

Electrode reactions on metallic electrodes in their pure molten salts are very fast because of the high temperature of the melt and the high concentrations of the reacting ions. For these reasons such electrode reactions are seen by most classical electroanalytical methods as reversible. The most suitable methods which can be applied for the determination of the kinetics of such very fast electrode reactions are the relaxation techniques. In this paper a combination of the relaxation [5, 6] and the faradaic impedance [8, 9] methods will be used.

It was shown in the previous papers [4, 10, 11], that the proper equivalent circuit to be used for the description of a reversible electrode in its pure molten salt, should contain, in addition to double layer capacitance, also an inductance. Such an equivalent circuit for a simple charge transfer reaction without diffusion is presented in Fig. 1(a), while Fig. 1(b) and (c) represent more complex circuits to be treated in the following.

Although the faradaic impedance method alone is basically capable of determining all the parameters of a given equivalent circuit, the charge transfer resistance of reversible electrodes in molten salts is too small to be measured accurately by this method. It is, however, necessary to add that the proper interpretation of the experimentally recorded impedance spectra of metal electrodes in pure molten salts is impossible without the use of the inductance.

If the reversible electrode described by the equivalent circuit presented in Fig. 1(a) is perturbed by a

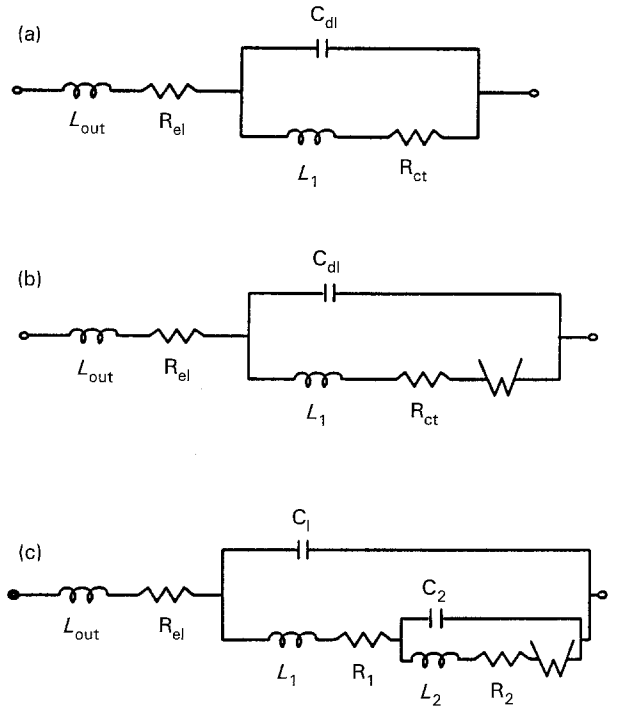

Fig. 1. Equivalent circuits.

galvanostatic current pulse, the resulting overpotential decay is described according to [5] by Equation 8:

$$\eta(t) = \frac{\eta(0)}{s_2 - s_1}(s_1 \exp(-s_2 t) - s_2 \exp(-s_1 t)) \quad (8)$$

with

$$s_1 = \frac{R_{ct}}{2L_1} + \left[\left(\frac{R_{ct}}{2L_1}\right)^2 - \frac{1}{C_{dl}L_1}\right]^{1/2} \quad (9)$$

$$s_2 = \frac{R_{ct}}{2L_1} - \left[\left(\frac{R_{ct}}{2L_1}\right)^2 - \frac{1}{C_{dl}L_1}\right]^{1/2} \quad (10)$$

where $\eta(0)$ is the overpotential at zero time ($t = 0$).

It follows from the form of the parameters s_1 and s_2 that they represent certain angular frequencies. The computer fit of the experimental relaxation curve can provide these two frequencies, but the two frequencies alone cannot provide all three parameters (C_{dl}, L_1 and R_{ct}) which describe the electrical double layer in the equivalent circuit presented in Fig. 1(a). Additional information (inductance or double layer capacitance) must be obtained from the faradaic impedance spectra. If this additional information from the frequency domain is the inductance (L_1), the charge transfer resistance (R_{ct}) is then calculated from

$$R_{ct} = L_1(s_1 + s_2) \quad (11)$$

The electrochemical technique providing the corresponding information in the frequency domain is electrochemical impedance spectroscopy, EIS [8, 9]. This has well established theory for typical equivalent circuits with electrolyte resistance, double layer capacitance, charge transfer resistance and Warburg diffusion impedance. Many other complications of electrode processes have also been considered theoretically and tested experimentally. Computer programs are available [12, 13] for the evaluation of the equivalent circuit parameters from the experimentally recorded complex electrochemical cell impedance.

The relaxation curve which results from a charge perturbation of a typical Randles equivalent circuit is given by the coulostatic method [14, 15]. The relaxation theory of an inductive electrode circuit presented in Fig. 1(b), which represents a high energy diffusive electrode reaction, was also derived recently [6] and is represented by

$$\eta(t) = A\exp(\alpha^2 t)\,\mathrm{erfc}\,(\alpha t^{1/2}) + B\exp(\beta^2 t)\,\mathrm{erfc}\,(\beta t^{1/2}) + C\exp(-\gamma t) \quad (12)$$

with

$$\eta(0) = A + B + C \quad (13)$$

$$R_{ct} = L_2(\alpha\beta + \gamma) \quad (14)$$

$$Z_d = L_2(\alpha + \beta)\gamma \quad (15)$$

It is important to notice that the parameters α, β and γ of Equation 12 may be used for the evaluation of the charge transfer resistance (Equation 14) and the Warburg diffusion impedance (Equation 15), providing the low frequency inductance L_2 is known from separate impedance spectroscopy measurements.

The analysis of the recorded impedance spectra over a wide frequency range should in fact itself (by a special nonlinear least squares fit (NLLS-fit)), produce all desired parameters of the equivalent circuit. However, as mentioned above, the determination of a small charge transfer resistance is not accurate enough, and much better results are obtained by a combination of these two methods.

With the assumption of the above mechanism, it should also be possible to fit the low frequency impedance spectra by the equations derived, for a preceding chemical reaction followed by a charge transfer step (CE), as given by several authors [16–18]:

$$Z_{per} = Z' - iZ'' \quad (16)$$

with

$$Z' = R_{ct} + \sigma_R\omega^{-1/2} + \frac{K}{1+K}\sigma_O\omega^{-1/2} + \frac{1}{1+K}\sigma_O\left[\frac{(\omega^2+k^2)^{1/2}+k}{\omega^2+k^2}\right]^{1/2} \quad (17)$$

$$Z'' = \sigma_R\omega^{-1/2} + \frac{K}{1+K}\sigma_O\omega^{-1/2} + \frac{1}{1+K}\sigma_O\left[\frac{(\omega^2+k^2)^{1/2}-k}{\omega^2+k^2}\right]^{1/2} \quad (18)$$

In the above expressions,

$$\sigma = \sigma_O + \sigma_R = \frac{RT}{n^2F^2A\sqrt{2}}\left(\frac{1}{D_R^{1/2}c_R^*} + \frac{1}{D_O^{1/2}c_O^*}\right) \quad (19)$$

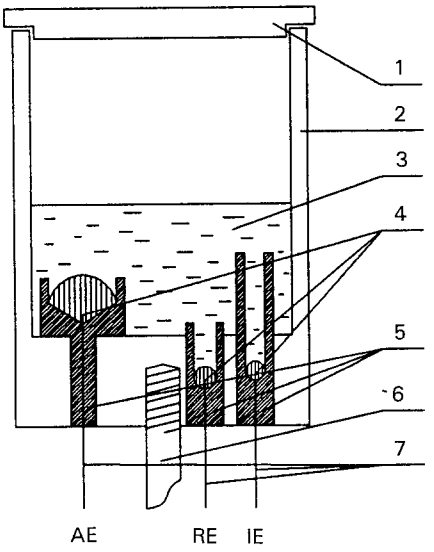

Fig. 2. The measuring cell. (AE) auxiliary, (RE) reference, (IE) indicator electrodes. (1) graphite cover, (2) graphite crucible, (3) cryolite–alumina melt, (4) liquid aluminium, (5) boron nitride, (6) supporting steel rod, (7) molybdenum wires.

is related to the Warburg impedance, and the meaning of k is

$$k = k_1 + k_2 \tag{20}$$

where k_1 and k_2 are the rate constants of the preceding chemical reaction, and

$$K = \frac{k_1}{k_2} \tag{21}$$

is the equilibrium constant of the preceding chemical reaction. The subscripts O and R refer to the oxidized and reduced species, respectively [8].

3. Experimental details

3.1. *Materials*

Crystals of hand-picked Greenland cryolite were used without further purification. The γ-Al_2O_3 was of analytical grade. All three electrodes were made up of super purity (99.99% Al) aluminium. Experiments were run in pure cryolite and in cryolite-alumina melts with 2, 4, 6, 8, 10 and 12 wt % Al_2O_3.

3.2. *Apparatus and procedure*

The experimental cell which was used for both relaxation and impedance measurements, is presented in Fig. 2. The indicator electrode area was 0.25 cm^2. The measuring cell was kept in dry argon in an electrically heated furnace with temperature control to ±0.2 K. The cell was equilibrated at a given temperature for at least 1 h.

A constant current pulse between the indicator and the auxiliary electrodes was supplied by a PAR model 173 potentiostat–galvanostat with a PAR model 175 universal programmer. The duration of the current pulse was always 0.1 ms. The current was chosen in such a way that the resulting overpotential perturbation at zero time did not exceed 30–50 mV. The relaxation of the overpotential of the working electrode (against the reference electrode) was recorded by a LeCroy LS140 scope station. The faradaic impedance spectra were recorded in the same measuring system using a computer controlled Solartron 1260 phase-gain analyser in a two electrode configuration at equilibrium potential.

4. Results

4.1. *High frequency results*

4.1.1. Impedance data. The evaluation of the inductance from the recorded impedance spectra requires recording over a broad frequency range. For this purpose faradaic impedance spectra were

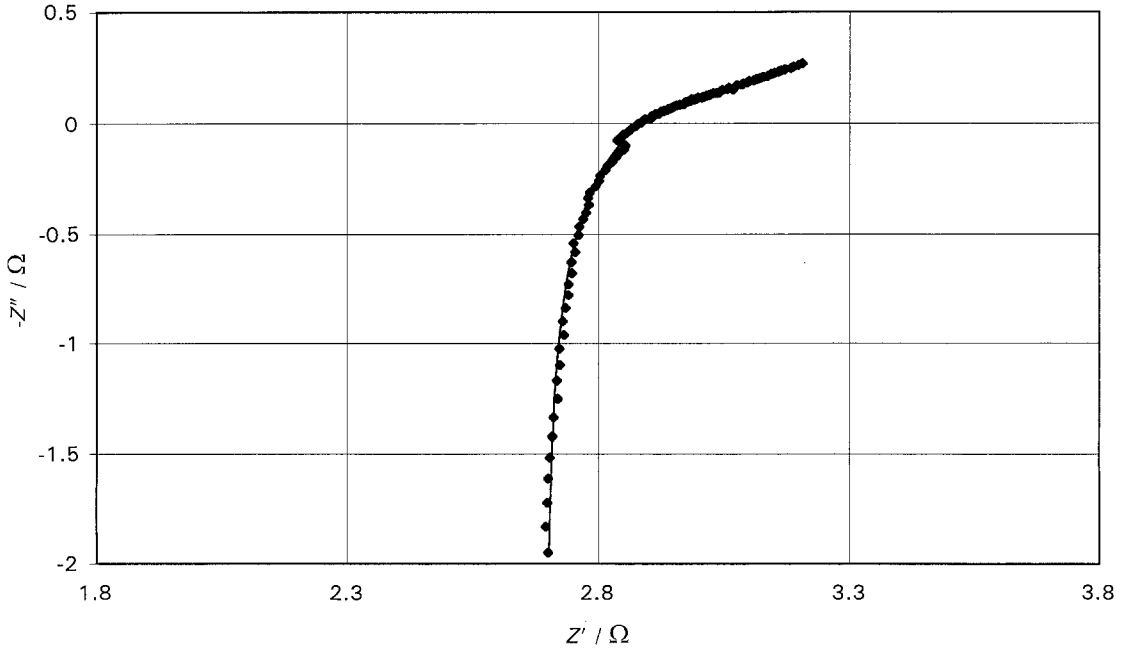

Fig. 3. Impedance spectrum of Al indicator electrode in a cryolite–2 wt % Al_2O_3 melt at 980 °C.

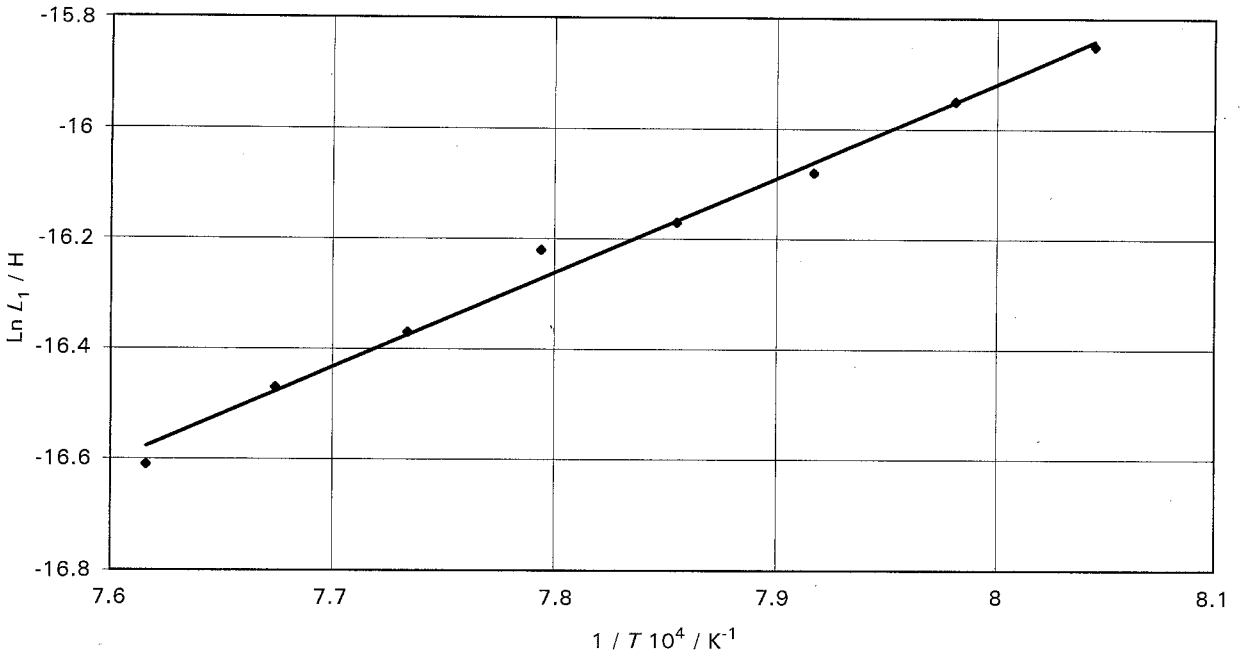

Fig. 4. Temperature dependence of the high frequency double layer inductance. The least squares equation of the straight line is $\ln L_1 = -29.638 + 17\,149/T$, with the determination coefficient $r = 0.995$.

recorded in the range from 10 Hz to 1 MHz (covering 400 frequencies). A typical recording together with the NLLS-fit obtained by Boucamp's program [12] is shown in Fig. 3. The description of the elements are as shown in Fig. 1(c). The outer inductance L_{out}, due to the original Solartron electrical cable used for the connection of the Solartron 1260 to the measuring cell, tungsten rods used for the electrode connection, electrical furnace etc., was $0.6 \pm 0.1\ \mu$H and was temperature independent.

The interpretation of the impedance spectra is based on the assumption that the electrode process on the aluminium electrode in cryolite–alumina solutions has to be treated as a three-step electrode process (i.e. a preceding chemical step, a low frequency step influenced by diffusion and a pure charge transfer at high frequency). For the two charge transfer processes the equivalent circuit presented in Fig. 1(c) should be used. The preceding chemical step involves computations based on Equations 17 and 18. Such fitting was performed for all the recorded impedance spectra (7 concentrations, for each concentration 5–7 temperatures, 3 spectra at each temperature), with the purpose of evaluating the high frequency (L_1) and low frequency inductances (L_2). It appeared that the high frequency inductance (L_1) was only temperature dependent, but did not depend on the concentration of alumina in cryolite. Similar to what was reported

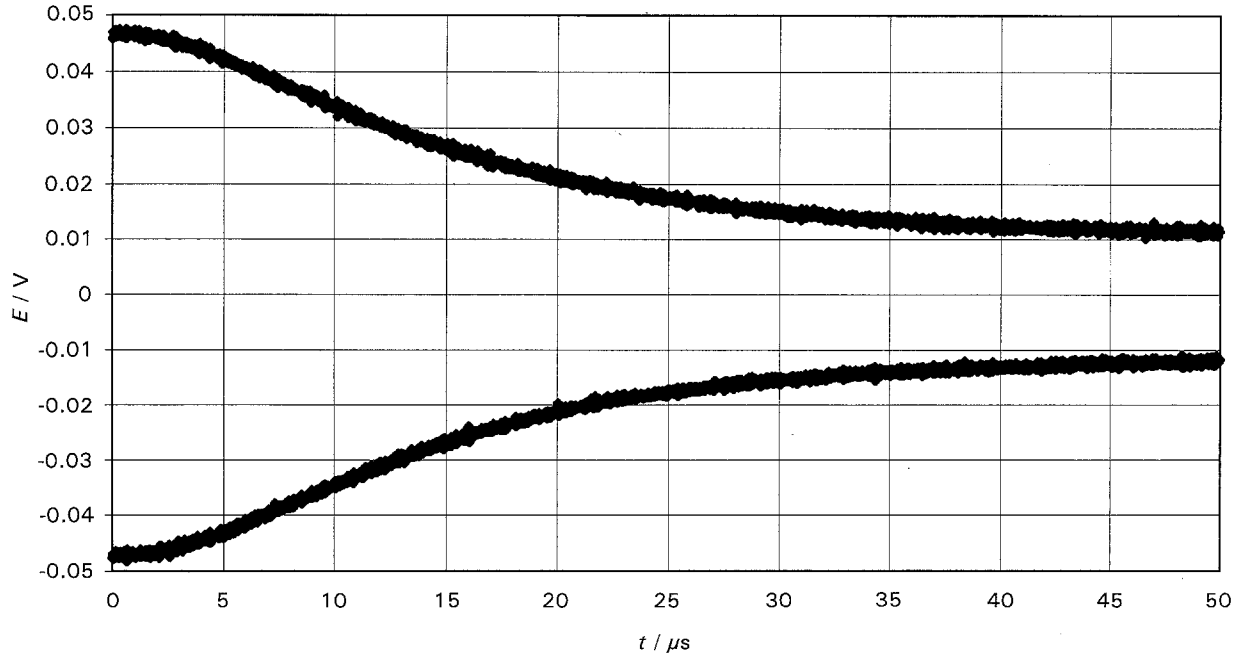

Fig. 5. Anodic and cathodic relaxation curves of the aluminium electrode in cryolite–4 wt % Al_2O_3 at 1000 °C. The value of the sum of the frequencies ($s_1 + s_2$), obtained by a special computer program, amounts to 313 000 s^{-1}.

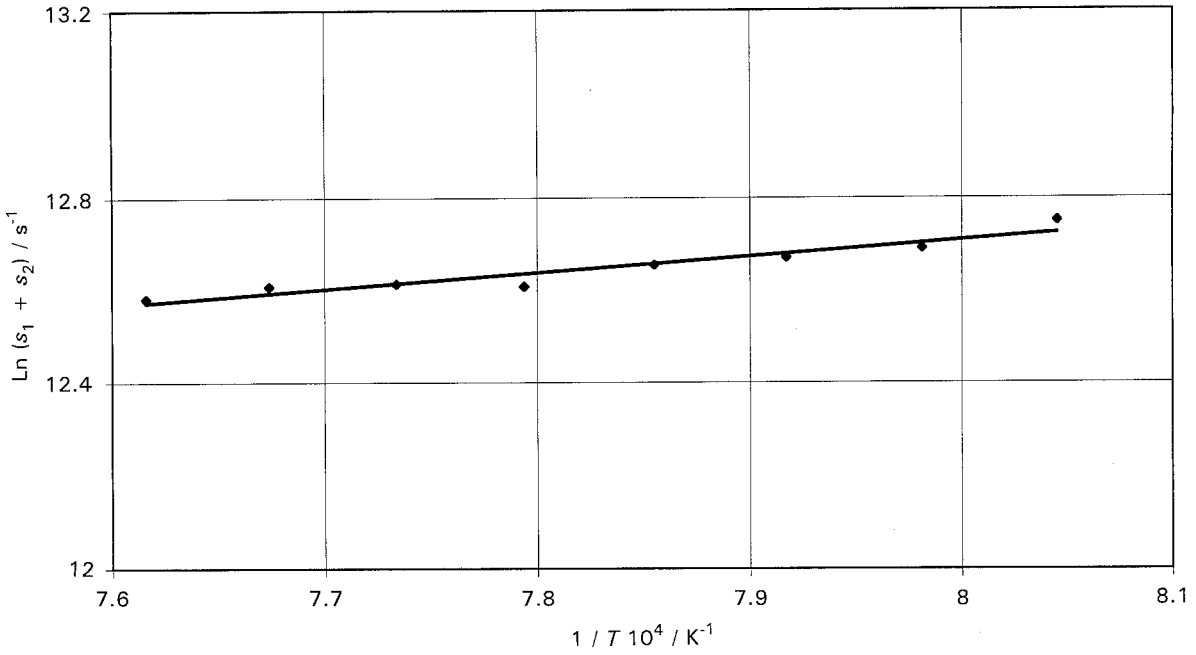

Fig. 6. Temperature dependence of the sum of angular frequencies ($s_1 + s_2$).

in our previous paper [4], the high frequency inductance depends exponentially on $1/T$. This dependence is presented in Fig. 4. The high frequency charge transfer resistance, R_1, can be calculated from the above high frequency inductance according to Equation 11, if the sum of the frequencies ($s_1 + s_2$) is known from relaxation measurements.

4.1.2. Relaxation results. The relaxation curve, corresponding to the discharge of the high frequency loop after a galvanostatic pulse, was located in the microsecond time range. The overpotential decay does not go to zero as there is still a second, diffusion dependent, low frequency relaxation process. For each concentration of alumina, four cathodic and four anodic relaxation curves were recorded, each curve being composed of 2000 points. Typical microsecond relaxation recordings are presented in Fig. 5.

Similar to the high frequency inductance, the sum ($s_1 + s_2$) also appeared to depend only slightly on temperature, but not on the alumina concentration. This dependence, as obtained from all microsecond relaxation curves, is presented in Fig. 6. With the value of the sum ($s_1 + s_2$) and the high frequency inductance, it is possible to calculate the high frequency charge transfer resistance, R_1, by means of Equation 11 and the corresponding exchange current density j_{04}:

$$j_0 = \frac{RT}{nFR_{ct}A} \tag{22}$$

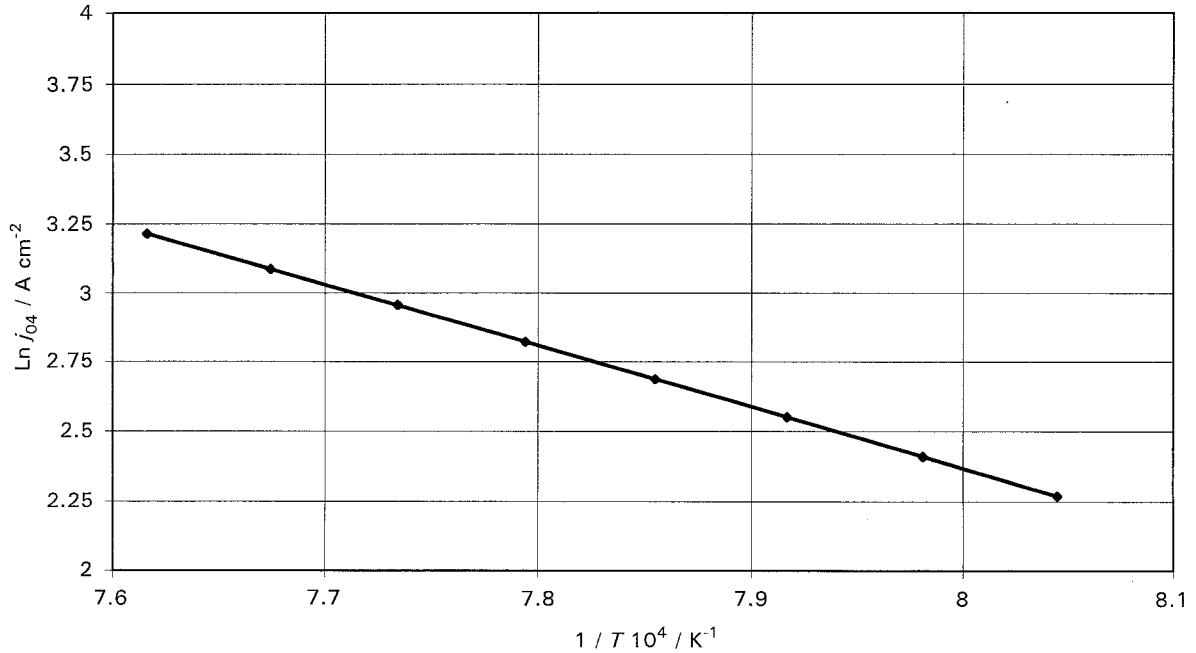

Fig. 7. Arrhenius plot of the exchange current density of step (Equation 4). The least squares equation of the straight line is $\ln j_{04} = 19.9564 - 21\,984/T$.

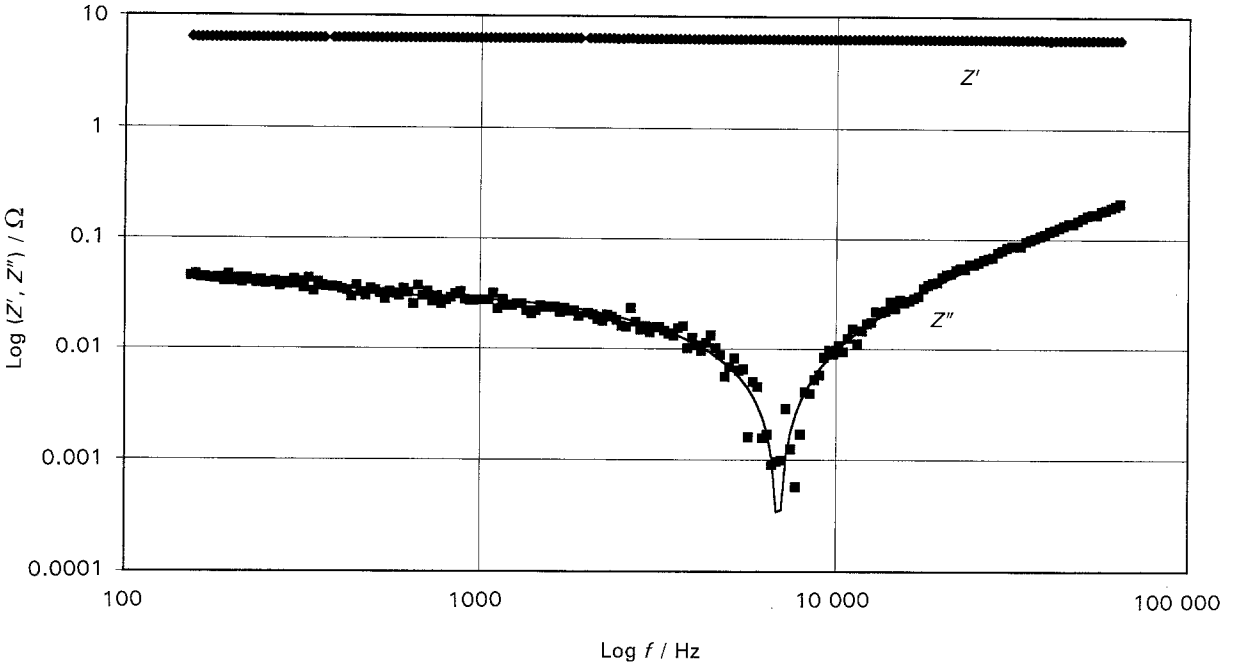

Fig. 8. Bode plot of an impedance spectrum together with the NLLS-fit for an aluminium electrode in cryolite–6 wt % of Al_2O_3 at 980 °C.

with $n = 1$ and the electrode area $A = 0.25\,cm^2$. The temperature dependence of the exchange current density step (Equation 4) is presented in Fig. 7 in the form of an Arrhenius type plot.

5. Low frequency results

In contrast to the high frequency inductance, all the low frequency parameters of the equivalent circuit appeared to be dependent not only on temperature, but also on the alumina concentration. For the evaluation of the charge transfer resistance step (Equation 3) and the Warburg diffusion impedance according to Equations 14 and 15, the most important parameter obtained from the fit of the impedance spectrum is the low frequency inductance and from the relaxation curves, the parameters α, β and γ.

The low frequency inductance was obtained by a computer fit of the recorded impedance spectra using Boucamp's program [12] according to the equivalent circuit presented in Fig. 1(c). Such a recording in the frequency range 100 Hz to 65 kHz is presented in the form of a Bode plot in Fig. 8 for a melt containing 6 wt % of the dissolved alumina. Markers represent the experimental points whereas the line presents the NLLS-Fit. The scatter of the experimental points is more pronounced in the frequency range where the imaginary part crosses the real axis and changes sign. The parameters α, β and γ of Equation 12 were obtained by a computer fit of the millisecond

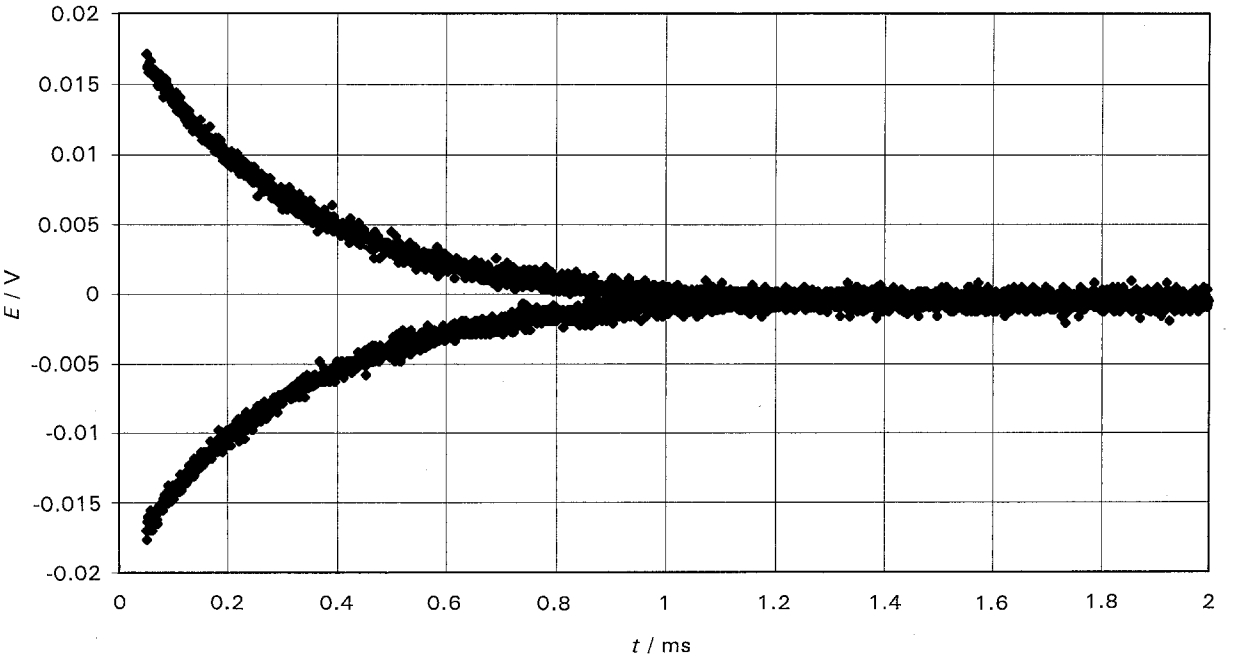

Fig. 9. Anodic and cathodic millisecond time range relaxation curves of an aluminium electrode in pure molten cryolite. 2000 points. Temperature 1010 °C.

Table 1. Low frequency data for pure cryolite

T /° C	L_2 /μH	α /$s^{-1/2}$	β /$s^{-1/2}$	γ /s^{-1}	R_2 /Ω cm^2	j_{03} /A cm^{-2}	Z_w /Ω $s^{-1/2}$
1010	1.96	306	191	3233	0.031	1.78	3.22
1020	1.22	262	188	3380	0.0160	3.48	1.81
1030	1.20	245	179	3220	0.0131	4.27	1.62
1040	1.05	165	190	3418	0.0096	5.89	1.29

Electrode area, $A = 0.25\,cm^2$.

time range relaxation curves. Such a recording is presented in Fig. 9. It should be noted, that the millisecond range relaxation curves in Fig. 9 do not start at zero time, because the microsecond relaxation time has been removed from the file. However, contrary to Fig. 5, the overpotential decay of the millisecond range relaxation time drops to zero. The low frequency results for pure cryolite are presented in Table 1. Similar tables were obtained for the six concentrations of alumina (2, 4, 6, 8, 10 and 12 wt %) in molten cryolite. The final results are presented in two graphs. Figure 10 shows Arrhenius plots of the exchange current densities of the step in Equation 7 in alumina-containing melts, and Fig. 11 depicts the dependence of the Warburg diffusion impedance upon the temperature for various alumina concentration. The constants A_1, B_1 and A_2, B_2 of the least squares equations

$$\ln j_{07} = A_1 - \frac{B_1}{T} \tag{23}$$

$$\ln Z_w = A_2 + \frac{B_2}{T} \tag{24}$$

are given in Table 2.

Table 2. Coefficients of the least squares Equations 23 and 24 for various concentration of alumina in molten cryolite

wt % Al_2O_3	A_1	B_1	A_2	B_2
0	50.479	63 882	−39.18	51 600
2	12.204	14 673	−5.327	8280
4	9.131	10 139	−4.575	6865
6	9.435	9874	−5.107	6907
8	9.503	9522	−5.343	7098
10	10.36	10 432	−3.674	4463
12	8.786	8255	−3.627	3830

6. The preceding chemical reaction

To evaluate the low frequency impedance spectra in terms of a preceding chemical reaction, the part of the impedance spectra corresponding to the high frequency step (Equation 3) (including outer inductance and the electrolyte resistance) was first subtracted by use of the DATA CRUNCHER in the EQUIVCRT program [12]. The remaining impedance spectrum was fitted by a special NLLS-fit program based on Equations 17 and 18 in the low frequency range. The results for several temperatures are presented in Table 3 for pure cryolite melt and for a cryolite–alumina melt.

7. Discussion

It follows from the above results that the mechanism of the aluminium electrode reaction in molten cryolite–alumina mixtures, proposed in our previous paper [4], can now be written by the following set of reactions. For pure molten cryolite,

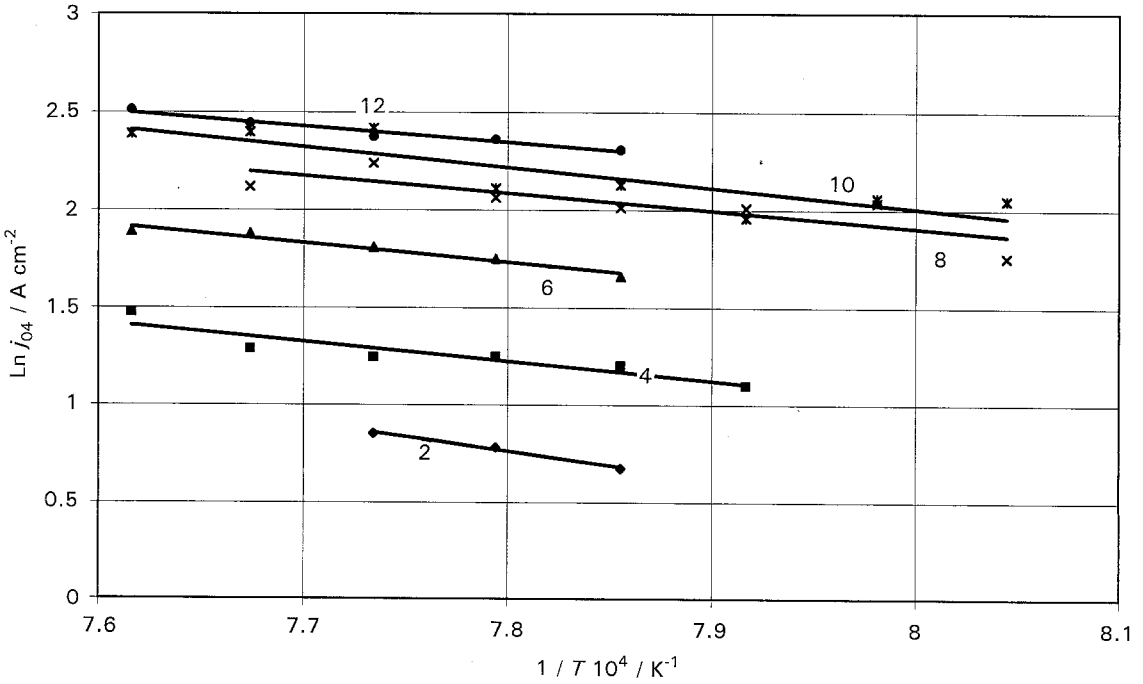

Fig. 10. Arrhenius plots of the exchange current densities of step (Equation 7) for different contents of alumina (wt %).

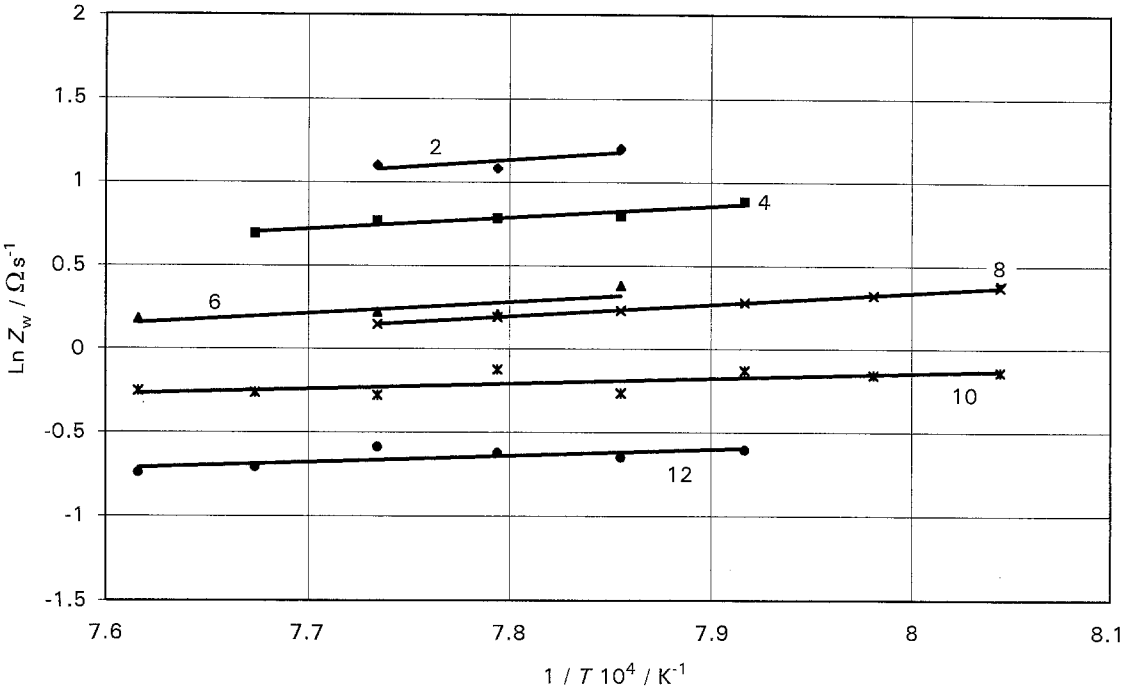

Fig. 11. Temperature dependence of the Warburg diffusion impedance for various contents of alumina (wt %).

$$AlF_6^{3-} \underset{k_2}{\overset{k_1}{\rightleftharpoons}} AlF_4^- + 2F^- \quad (5)$$

$$AlF_4^- + 2e^- = AlF_{2(ads)} + 2F^- \quad (3)$$

$$AlF_{2(ads)}^- + e^- = Al + 2F^- \quad (4)$$

In cryolite–alumina melts, the aluminium oxyfluoride complexes take part in the electrode process:

$$Al_2OF_6^{2-} \underset{k_2}{\overset{k_1}{\rightleftharpoons}} Al_2OF_4 + 2F^- \quad (6)$$

$$Al_2OF_4 + 2e^- \Longleftrightarrow AlF_{2(ads)}^- + AlOF_2^- \quad (7)$$

$$AlF_{2(ads)}^- + e^- = Al + 2F^- \quad (4)$$

The suggestion, however, given in our previous paper, that the charge transfer step (Equation 3) also occurs in pure cryolite melt, is now confirmed, as it was possible to determine its exchange current density.

New results were provided by the concept of a preceding chemical reaction. It should be pointed out that the dissociation reaction (Equations 5 and 6) do not exactly correspond to the type of reactions assumed in the derivation of Equations 17 and 18 (i.e. a first order preceding reaction) but in spite of this, the results of the equilibrium constant agree fairly well with the literature values [1]. The degree of dissociation of the AlF_6^{3-} ion at 1000 °C according to Equation 5 is ~ 0.25 [1], which corresponds to an equilibrium constant of 0.08. The addition of alumina does not seem to have a great influence upon the equilibrium constant, but the sum of the homogeneous rate constants k (Equation 20) increases in the alumina-containing melts, as compared to pure molten cryolite (Table 3). Another interesting conclusion may also be drawn from the Warburg coefficients σ_R and σ_O presented in Table 3. The value of the Warburg coefficient corresponding to the reduced species, σ_R, which, according to the proposed mechanism, is the same in all melts (AlF_2^-), is almost equal in pure cryolite and in 12 wt % solution of alumina. The addition of alumina, however, increases the Warburg coefficient of the oxidised species, which in pure cryolite melt is AlF_4^-, but changes to a more bulky oxyfluoride species (e.g. Al_2OF_4) in cryolite–alumina melts. Another strong support for the mechanism represented by the above equations comes from the value of the charge transfer coefficient, α_c. Its value, as calculated by the method given by Bockris and Reddy [19] amounts to 1. For the transfer step (Equation 7), the exchange current density is given by

$$j_{07} = 2k^0 c_{Al(III)}^{\alpha_c} c_{Al(I)}^{\alpha_a} c_{AlOF_2^-} \quad (25)$$

from which the cathodic charge transfer coefficient corresponds to the slope:

Table 3. Data based on a preceding chemical reaction in a pure cryolite melt and at 12 wt % dissolved in alumina at various temperatures

T/°C	$\sigma_R/\Omega s^{-1/2}$		$\sigma_O/\Omega s^{-1/2}$		K		k/s^{-1}	
	cr	*cr + alumina*	*cr*	*cr + alumina*	*cr*	*cr + alumina*	*cr*	*cr + alumina*
1010	0.80	1.0	2.9	6.2	0.17	0.13	2100	8000
1020	0.75	0.95	3.0	7.0	0.18	0.16	1850	7300
1030	0.86	0.90	2.6	6.7	0.21	0.17	1500	5700
1040	0.80	0.80	2.9	5.9	0.23	0.21	1300	5250

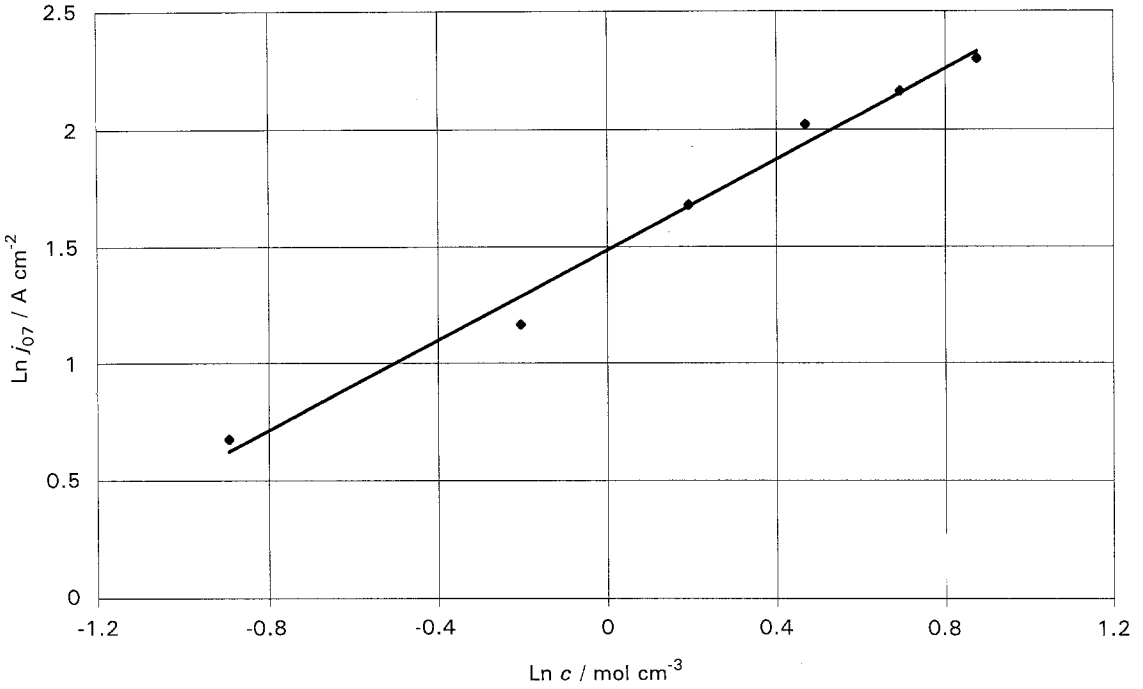

Fig. 12. The evaluation of the cathodic charge transfer coefficient α_c of the charge transfer step (Equation 7). The least squares straight line equation is: $\ln j_{07} = 1.486 + 0.964 \ln c_{Al_2O_3}$.

$$\frac{\partial \ln j_{07}}{\partial \ln c_{Al(III)}} = \alpha_c \qquad (26)$$

Such a plot is presented in Fig. 12, where the slope of the least squares straight line, 0.964, is, within the experimental error of ±0.05, equal to 1. That is another confirmation of the proposed mechanism.

It was stated above, that the change from a pure cryolite melt to alumina-containing melts is accompanied by the formation of more bulky oxyfluoride anionic complexes. After addition of alumina the activation energy of the charge transfer step, taken from Table 2 ($E_A = RB_1$) drops remarkably (Fig. 13) from about 530 kJ mol^{-1} in pure cryolite to around 86 kJ mol^{-1} in alumina-containing melts. It is thus obvious that the discharge of the aluminium oxyfluoride complex anion is much easier than that of the aluminium tetrafluoride anion. This can be, however, better understood in the light of the kinetics of the preceding chemical reaction, whose rate constants greatly increases by the addition of alumina as shown in Table 3.

The charge transfer step (Equation 4), the rate of which is expressed by the exchange current density j_{04}, appeared to be independent of the alumina concentration. The activation energy of that step

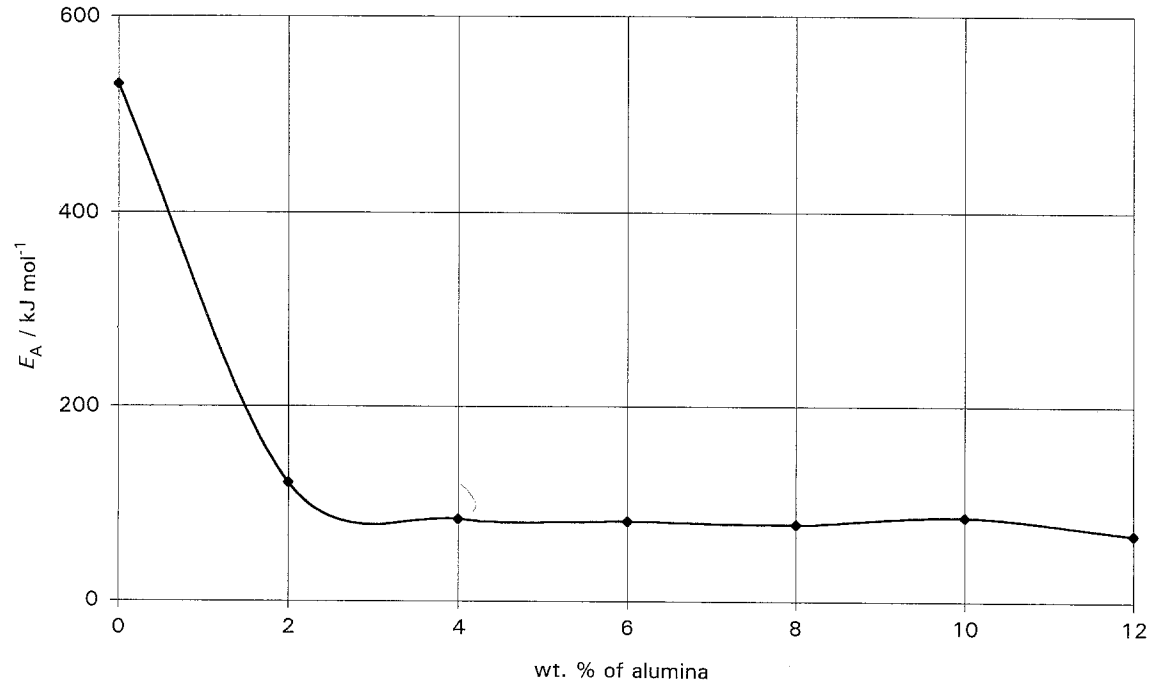

Fig. 13. Concentration dependence of the Arrhenius activation energy of the charge transfer step (Equation 7).

($\sim 183\,kJ\,mol^{-1}$, see Table 2, $E_A = RB_1$) indicates that the discharge does not go from a simple Al(I) cation. In the latter case the activation energy would have been much smaller.

8. Conclusions

The mechanism of the aluminium electrode reaction in pure molten cryolite and in alumina containing cryolite melts can be described as a three-step process: two charge transfer reactions preceded by a dissociation reaction. In pure molten cryolite this preceding reaction may be the dissociation of the hexafluoroaluminium anion, whereas in alumina containing melts a more bulky oxyfluoride anion is involved. The first charge transfer step which above has been referred to as the low frequency step is connected with diffusion and its exchange current density ranges from $1.97\,A\,cm^{-2}$ for 2 wt % to $9.98\,A\,cm^{-2}$ for 12 wt % of alumina at 1000 °C. A dramatic change of the activation energy for this charge transfer step is observed between pure molten cryolite ($E_A = 530\,kJ\,mol^{-1}$) and alumina containing melts ($E_A = 86\,kJ\,mol^{-1}$). The exchange current density of the second charge transfer step, which is alumina concentration independent, is much higher ($14.7\,A\,cm^{-2}$ at 1000 °C) and its activation energy ($E_A = 183\,kJ\,mol^{-1}$) indicates that a complex ion, most probably AlF_2^- is discharged.

Acknowledgements

Financial support from the Norwegian Research Council is gratefully acknowledged.

References

[1] J. Thonstad, 'Aluminium electrolysis, electrolyte and electrochemistry', *in* 'Advances in molten salt chemistry', Vol. 6. (Edited by G. Mamantov *et al.*), Elsevier, Amsterdam (1987) p. 73.
[2] J. Thonstad and S. Rolseth, *Electrochim. Acta* **23** (1978) 223, 233.
[3] R. Piontelli and G. Montanelli, *Alluminio* **25** (1956) 79.
[4] J. Thonstad and A. Kisza, 'Molten salt forum' Vol. 1–2, Trans. Tech. Publications, Aldermannsdorf, Switzerland (1993/94) p. 195.
[5] A. Kisza, *Polish J. Chem.* **67** (1993) 885.
[6] *Idem*, *ibid.* **68** (1994) 613.
[7] J. R. Macdonald, Private communication. Department of Physics and Astronomy, University of North Carolina, Chapel Hill, NC.
[8] J. A. Bard and R. L. Faulkner, 'Electrochemical methods, fundamentals and applications', John Wiley, New York (1980).
[9] J. R. Mcdonald, 'Impedance spectroscopy', John Wiley, New York (1987).
[10] A. Kisza and J. Kazmierczak, *Polish J. Chem.* **68** (1994) 329.
[11] A. Kisza, J. Kazmierczak, B. Borresen, G. M. Haarberg and R. Tunold, *J. Electrochem. Soc.* **142** (1995) 1035.
[12] B. Boucamp, 'Equivalent circuit', University of Twente, Holland (1988/89).
[13] J. R. Macdonald, Complex non-linear least squares immittance fitting program, Department of Physics and Astronomy, University of North Carolina, Chapel Hill, NC.
[14] P. Delahay, *J. Phys. Chem.* **66** (1962) 2204.
[15] W. H. Reinmuth and C. E. Wilson, *Anal. Chem.* **34** (1962) 1159.
[16] D. E. Smith, 'Electroanalytical chemistry' Vol. 1, (edited by A. J. Bard), Dekker, New York (1966) p. 1.
[17] M. Sluyters-Rehbach and J. H. Sluyters, 'Electroanalytical chemistry', Vol. 4, (edited by A. J. Bard), Dekker, New York (1970) p. 1.
[18] H. Matsuda, P. Delahay and M. Kleinermann, *J. Am. Chem. Soc.* **81** (1979) 6379.
[19] J. O'M. Bockris and A. K. N. Reddy, 'Modern aspects of electrochemistry', Vol. 2, Plenum Press, New York (1970) pp. 1004–1008.